Direct Evidence for Diverse Source Complexity in Small Earthquakes (Mw3.3-5.0) Obtained from Short-Range Borehole Seismic Data

Keisuke Yoshida

Research Center for Prediction of Earthquakes and Volcanic Eruptions, Graduate School of Science, Tohoku University, Sendai, Japan

Corresponding author: Keisuke Yoshida, Research Center for Prediction of Earthquakes and Volcanic Eruptions, Tohoku University, 6-6 Aza-Aoba, Aramaki, Aoba-Ku, Sendai, 980-8578, Japan (keisuke.yoshida.d7@tohoku.ac.jp)

Key Points (<140 characters)

1. Short-range (< 8 km) seismic waveforms at an excellent seismic sensor clearly show the diversity in the complexity in 64 Mw3.3-5 events.
2. Even conservatively estimated, approximately 30% of the events had multiple pulses that differed significantly from simple source models.
3. Methods that account for complexity rather than those that assume an a priori source pattern are required to characterize small events.

Abstract (150 ≤ 150 words)

A good understanding of the rupture patterns of small earthquakes is essential to understand the differences between earthquakes of different sizes. However, resolving the source complexity of small events (Mw<5) is challenging, because their seismic waveforms are distorted during propagation. In this study, we used high-quality seismic waveforms recorded by an excellent downhole sensor in Japan to directly examine the source complexities of 64 Mw3.3-5.0 short-range earthquakes (< 8 km). We found that even the waveforms of microearthquakes (Mw < 2) were simple at the sensor, indicating that the waveforms were scarcely disturbed by structural inhomogeneities. We inferred the moment rate functions from the shapes of the direct P-waves, which showed diversity in their complexity. Even conservatively estimated, 30% of the events had multiple subevents. The results suggest that methods that account for complexity, rather than those that assume a simple source pattern, are required to characterize even small earthquakes.

Plain language summary (190 ≤ 200 words)

It has been established that the source parameters of small earthquakes is similar to that of large earthquakes. This suggests that small earthquakes (M<5) may have a similar degree of complexity as large earthquakes. However, the complexity of small earthquake ruptures is usually masked by the propagation effect on seismic waveforms. In many cases, the source parameters of small earthquakes are determined based on a model that assumes that they are simple without any real complexity. To evaluate how often complex ruptures of small earthquakes occur, high-quality seismic waveforms recorded by an excellent downhole sensor in Japan for 64 M3.3-5.0 short-range earthquakes (< 8 km) were used. We confirmed that the waveforms recorded at this sensor are only slightly distorted by propagation, directly showing the source process of the M3.3-5.0 earthquakes. The shapes of the direct P-waveforms show that their source processes are diverse and that more than 30 percent of the events have multiple subevents, unlike in commonly-used simple source models. This suggests that the characterization of small earthquakes may require quantities such as radiated seismic energy, which can be directly estimated even when complex ruptures are considered.

1. Introduction

To fully understand earthquakes, information on the time history of the radiation process is necessary. Moment-rate function (MRF) supplies essential information on earthquake source processes. Many researchers have retrieved the MRFs of major earthquakes (Mw>7) and several MRF databases have been constructed for large earthquakes, revealing the diversity of their ruptures (Tanioka & Ruff, 1997; Vallée et al., 2011; Ye et al., 2016). However, for small earthquakes (Mw<5), the retrieval of MRFs is challenging because propagation effects strongly influence their waveforms.

Because of the difficulty in reliably estimating their details, the source parameters for small earthquakes are often estimated using simple source process models. Precisely, the stress drop of an earthquake is estimated based on the corner frequencies of the ω^2 source spectra of Aki (1967) and Brune (1970) with some pre-assumed source models. Such models include those of Brune (1970), Sato and Hirasawa (1973), Madariaga (1978), and Kaneko and Shearer (2014). The assumptions in the above approaches include that earthquake rupture is characterized by a simple, single pulse. It is critical to verify the validity of these assumptions.

Previous studies have established that earthquake rupture patterns are remarkably similar for small and large earthquakes. Specifically, they reported that the stress drop (e.g., Kanamori & Anderson, 1975) and moment-scaled radiated energy (e.g., Ide & Beroza, 2001) are nearly constant, regardless of the static size of the earthquake. Still, debate continues as to whether or not the moment-scaled radiated energy is scale dependent (e.g., Abercrombie, 1995; Mayeda & Walter, 1996; Izutani & Kanamori, 2001; Ide & Beroza, 2001; Pérez-Campos & Beroza, 2001; Prejean & Ellsworth, 2001; Takahashi et al., 2005; Mayeda et al., 2005; Baltay et al., 2010; Malagnini et al., 2014; Nishitsuji & Mori, 2014; Zollo et al., 2014; Denolle & Shearer, 2016; Ye et al., 2016; Chounet et al., 2018). If the earthquake rupture is self-similar and independent of its static size, small earthquakes may have a similar degree of complexity as large earthquakes. Based on the empirical Green's function (EGF) approach (Mueller, 1985; Hough et al., 1997), several recent studies have shown that the MRFs of small earthquakes have multiple pulses and a certain complexity (Courboulex et al., 1996; Kwiatek, 2008; Holmgren et al., 2019;

Pennington et al., 2023; Yoshida & Kanamori, 2023). Pennington et al. (2023) reported that 60-80% of M2.6-3 events in the Pardfield area produced complex ruptures based on the EGF approach. This EGF approach is almost the only method available for retrieving the MRFs of small earthquakes (Mw<5). However, there is a risk of noise in the EGF, and differences in reflected waves owing to slight differences in locations and focal mechanisms can inadvertently make the MRFs appear more complex than they really are.

The most direct way to evaluate the complexities of MRFs is to directly examine the displacement waveforms (Kikuchi & Ishida, 1988; Kanamori et al., 1990; Houston et al., 1998; Harrington and Brodsky, 2009; Lin et al., 2016). This approach is simple but unaffected by potentially problematic assumptions when dealing with EGFs, such as neglegilbe differences in path effects and focal mechanisms (Hutchings & Viegas, 2012), noise in EGFs, and frequency-band limitations. Kanamori et al. (1990) showed that the 1988 Pasadena M_L4.9 event caused a two-pulse rupture based only on the waveforms at a short-range single station (4 km). Kikuchi and Ishida (1988) used a similar approach to examine the diversity in the shape of the MRFs of deep (z>50 km) earthquakes in Japan from far-field P-waves. However, earthquake waveforms are typically affected by propagation and site effects. The former effects (attenuation and scattering) become more dominant with increasing source distances and frequencies. Because of their short rupture durations and the need to investigate high frequencies, the MRFs of small earthquakes (Mw<5) cannot be captured by observations at typical observation distances (> 20 km). Additionally, soft near-surface sedimentary layers and heterogeneous velocity structures strongly distort seismic waveforms. The use of a downhole sensor surrounded by hard rocks with minimal amplification and attenuation is essential for retrieving source signals. However, few situations exist in which these conditions are met.

In northern Ibaraki Prefecture, Japan, the National Research Institute for Earth Science and Disaster Resilience (NIED) Hi-net operates an excellent borehole seismic station (N.JUOH), which helps to investigate this issue. The downhole sensor of this station is confined by granite rock with high velocity (Vp=5.4 km/s, Vs=3.2 km/s; https://www.kyoshin.bosai.go.jp/cgi-bin/kyoshin/db/siteimage.cgi?0+/IBRH14+kik+pdf), and the site amplification effect can be well taken into account. Intense seismicity has

occurred in this region since the 2011 M9 Tohoku earthquake (Fig. 1; more than 50,000 earthquakes of $M_{JMA} \geq 1$; Yoshida et al., 2015 and 2019), and this downhole sensor has recorded many earthquake waveforms within ten kilometers.

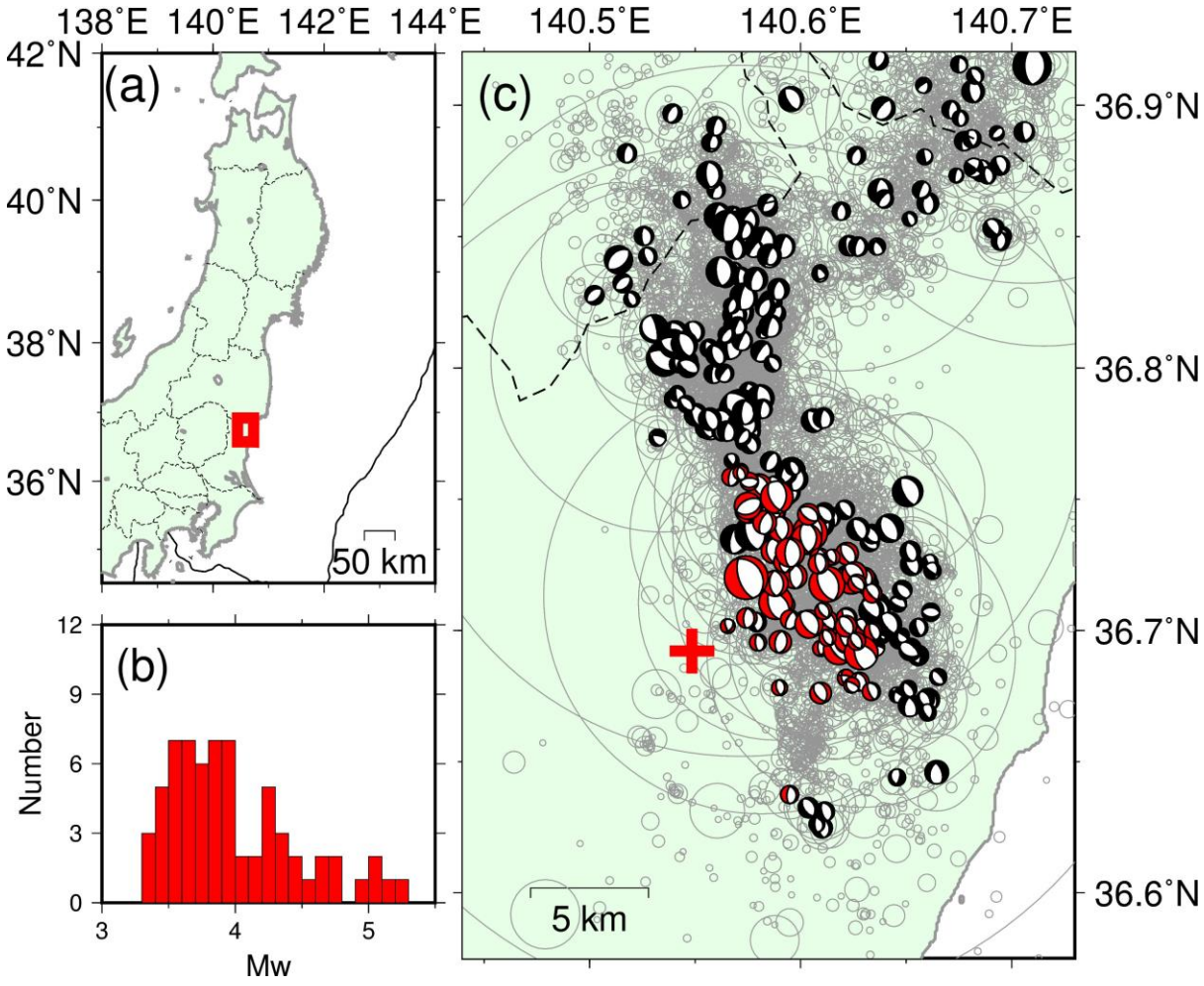

Figure 1. (a) Map showing the location of the study region. The red rectangle indicates the area shown in Fig. (c). (b) Histogram of Mw of the earthquakes to be analyzed. (c) Map showing the study region. The red cross denotes the station (N. JUOH) whose waveforms are analyzed in this study. The beach-balls represent the earthquake focal mecanisms listed in the F-net moment tensor catalog (Kubo et al., 2002), with red ones showing the events to be analyzed. Gray circles show the hypocenters of shallow earthquakes (z < 40 km) with the JMA magnitude $M_{JMA} \geq 2.0$ from January 1, 2003, to September 30, 2022. The circle sizes correspond to the diameters of Eshelby's (1957)

circular fault with a stress drop of 3 MPa.

This study examines the diversity of the MRFs of small earthquakes (Mw3.3-5.0) based on the close-range waveforms of direct P-waves. To evaluate the propagation effect, which is a problem when looking directly at waveforms, we referred to the waveforms of small earthquakes and synthetic waveforms based on a simple one-dimensional structure. A comparison of the observed waveforms with their synthetic counterparts helps evaluate the effects, including the geometrical spreading and surface reflections above the downhole sensor.

2. Characteristics of Observed Waveforms

Figure 2 shows the observed vertical components of the displacement waveforms for three events. The seismometer was a 1 Hz velocity meter, and we removed the instrument responses. The waveforms were very clean because of the short distances and hard bedrock conditions The first waveform is for the M_{JMA}1.4 event, high-pass filtered at 0.8 Hz to account for signal-to-noise ratio (Figs. 2a). The second and third correspond to M_{JMA}3.5 and M_{JMA}4.4, respectively, high-pass filtered at 0.12 Hz (Figs. 2b-c). The second waveform was recorded at a horizontal distance of 1.7 km from the hypocenter and the contributions of intermediate and near-field terms between the onsets of P and S waves (Fig. 2b). The P-waveform of the first event shows two pulses of approximately 0.04s apart (pink area in Fig. 2a), which represent waves that arrived directly at the downhole sensor and waves that arrived after being reflected by the ground surface directly above.

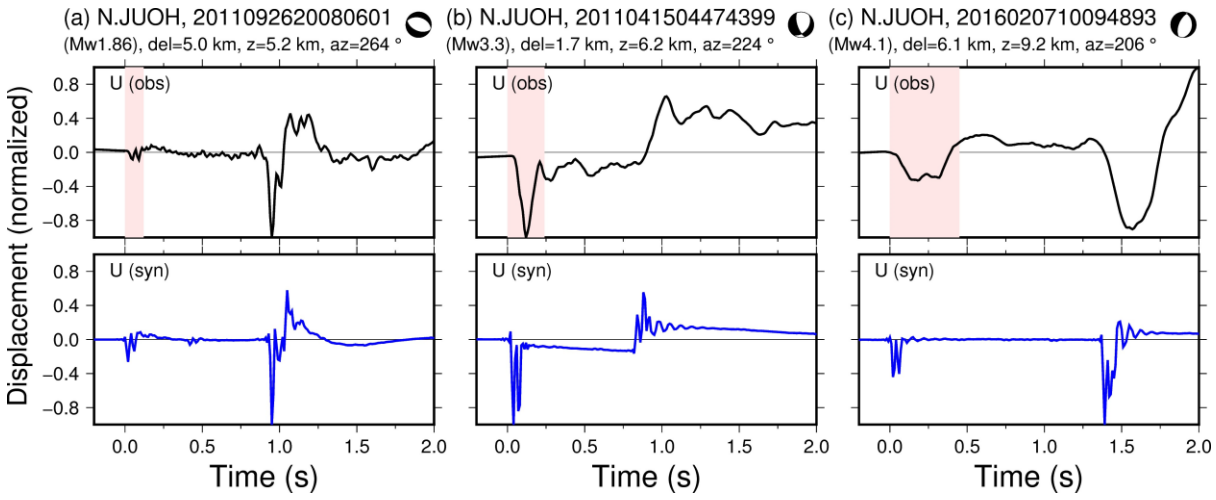

152

153 **Figure 2.** Displacement waveforms of three events obtained at the station to be used
154 (N.JUOH) and the synthetic waveforms. Above: observed waveforms. Bottom: synthetic
155 waveforms. The pink area indicates the direct P wave. The synthetic waveforms were
156 estimated using the moment tensors estimated in this study, shown in this figure. The
157 timing at which t=0 represents the onset of the P-wave.

158

159 The use of synthetic waveforms is helpful for evaluating the propagation effects.
160 The code of Zhu and Rivera (2002), based on the wavenumber integration method, was
161 used to compute synthetic waveforms. The assumed seismic wave velocity structure is
162 Hasegawa et al. (1978), used in routine processing at Tohoku University. Based on the
163 NIED Hi-net logging information, the velocities in the shallow 10 m was changed. The
164 empirical relationship proposed by Brocher (2008) was used to assume depth-dependent
165 density and Q structures (Fig. S1) following the procedure described by Yamaya et al.
166 (2022). The source duration was set to 0.01s to obtain the impulse response. The moment
167 tensors for M_{JMA}3.5 and M_{JMA}4.4 events were obtained from the F-net catalog (Kubo et
168 al., 2002). The moment tensor solution for the M_{JMA}1.4 event was estimated by taking the
169 amplitude ratios of nearby earthquakes listed in the nearby F-net moment catalog, based
170 on the method of Yoshida et al. (2019).

171 The synthetic waveforms (vertical displacements) for these three events are shown
172 in Fig. 2. These results agree well with the characteristics of the observed waveforms.
173 The agreement for the M_{JMA}1.4 (Mw1.9) event at such high frequencies supports our
174 assumption that these short-range data are scarcely disturbed by structural

inhomogeneities. A comparison between the observed spectrum of the P wave of this event and that of the synthetic one showed no systematic deviations (Fig. S2a). Although there are slight deviations reflecting the incompleteness of the structural model, they are negligible when discussing the macroscopic shape of the MRFs.

The details differ between the observed and synthetic waveforms for M_{JMA} 3.5 and 4.4 events because the synthetic waveforms do not include the effects of the MRFs (Figs. 2b-c). Reflecting this finiteness, the spectra of the observed waveforms of the two events deviate from the synthetic spectra to smaller values above a certain frequency (corner frequency) (Fig. S2b, c). This difference can be attributed to the effects of the MRFs on these events.

3. Complexity of moment-rate functions of 64 Mw3.3-5.0 events

Figure 3 shows the P-wave displacement waveforms of the vertical component for 1.0 s for 64 target events. A high-pass filter (cutoff frequency of 0.5 Hz) was applied, and the signs were adjusted to make the first onset positive. Waveforms for longer windows (2.5 s) are shown in Fig. S3. The shapes of the direct P-waves show diversity; some are simple, consisting of a single pulse (gray), whereas others are more complex (blue).

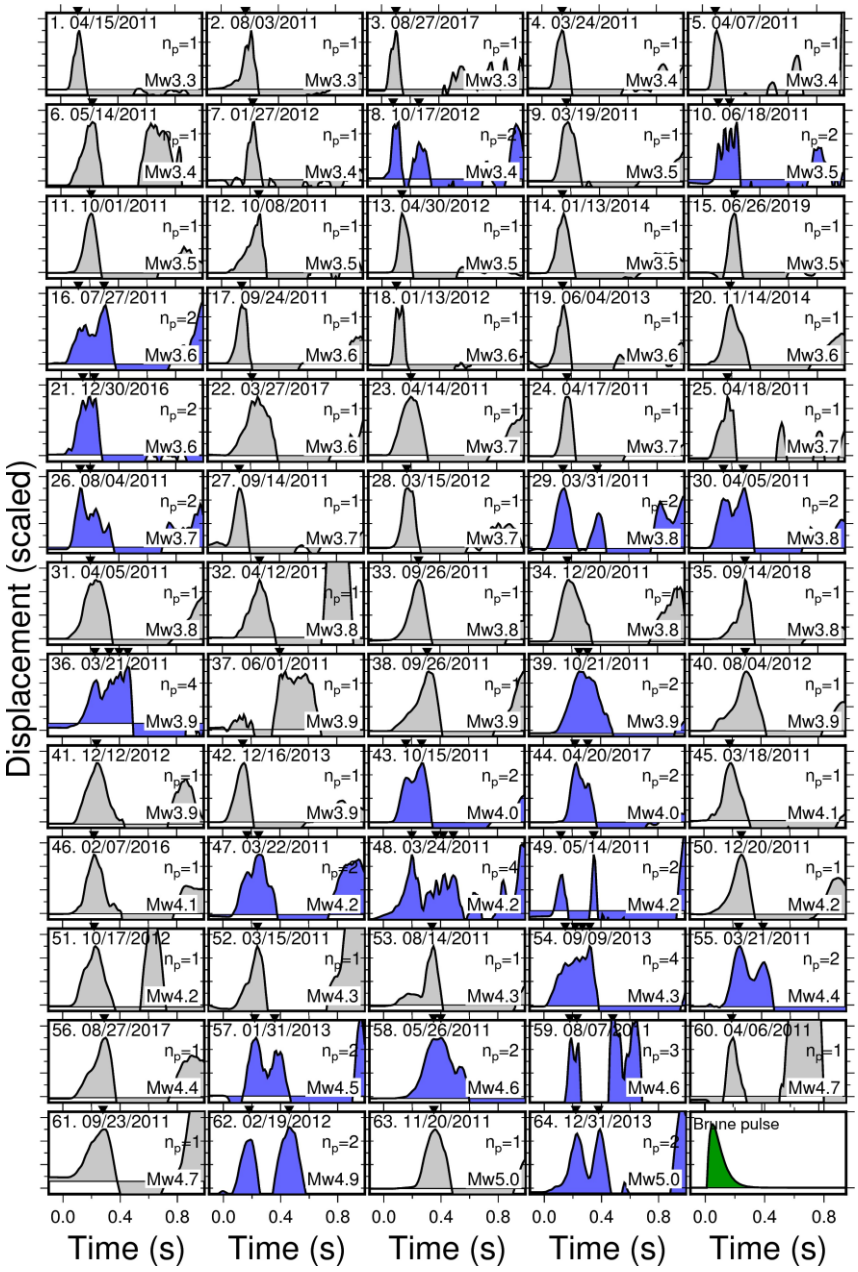

Figure 3. Enlargement of direct P-waves for 64 M_W3.3-5.0 earthquakes. They are arranged in order of Mw from smallest to largest. Triangles indicate the peaks of detected subevents. n_p indicates the number of detected subevents. The waveforms are shown in blue for earthquakes with more than two subevents. The lower right panel shows the MRF of Brune's (1970) model.

Given that the displacement waveform of the far-field P-wave is proportional to the MRF, this diversity may directly represent the diversity in the source process. In contrast,

the waveforms of the small earthquakes (M_{JMA}<2) occurring in the vicinity (within 1 km) of each earthquake were simple and similar, with essentially one pulse (Fig. S4). There were exceptions with two short-interval pulses (<0.04s) due to surface reflections, as shown in Fig. 2(a). This downhole sensor is located at a depth of 100 m. Therefore, two pulses are naturally observed owing to surface reflection. The synthetic waveforms computed at the location of each target event always had two pulses (Fig. S5). This effect appears mainly at > 20 Hz and almost disappears when a 20 Hz low-pass filter is applied (Fig. S6). Based on the empirical relationship of earthquakes in global settings by Duputel et al. (2013), the centroid time of an Mw2 event is approximately 0.028 s, which may mask two pulses owing to surface reflection. The presence of surface reflections limits the minimum duration of the MRFs inferred from direct inspection of the P-wave to approximately 0.1 s.

The durations of the direct P-waves of the Mw 3.3-5.0 events are longer than 0.1 s (Fig. 3). It is reasonable to assume that the diversity of the obtained P-waveforms of Mw3.3-5.0 events represents the diversity of the MRFs. Following Houston et al. (1998), we measured the complexity using the number of subevents in the time function before the S-wave arrival. The number of bumps was determined by the number of times the time derivatives of the waveforms crossed zero. We imposed the following conditions to avoid counting minor peaks due to surface reflections or noise: (1) The peak amplitude must be greater than 50% of the amplitude of the maximum peak. (2) The time interval between peaks should be greater than 0.05s. (3) The elapsed time from the previous peak should be less than 0.5 s. Fig. 4(a) shows the histogram of the number of subevents thus obtained. For 42 of the 64 events, the number of subevents was one, whereas for 22 events, the number of subevents was two or more. Even when the observed waveforms of Mw3.3-5 were low-pass filtered at 20 Hz, little change was observed in this trend (Fig. S7).

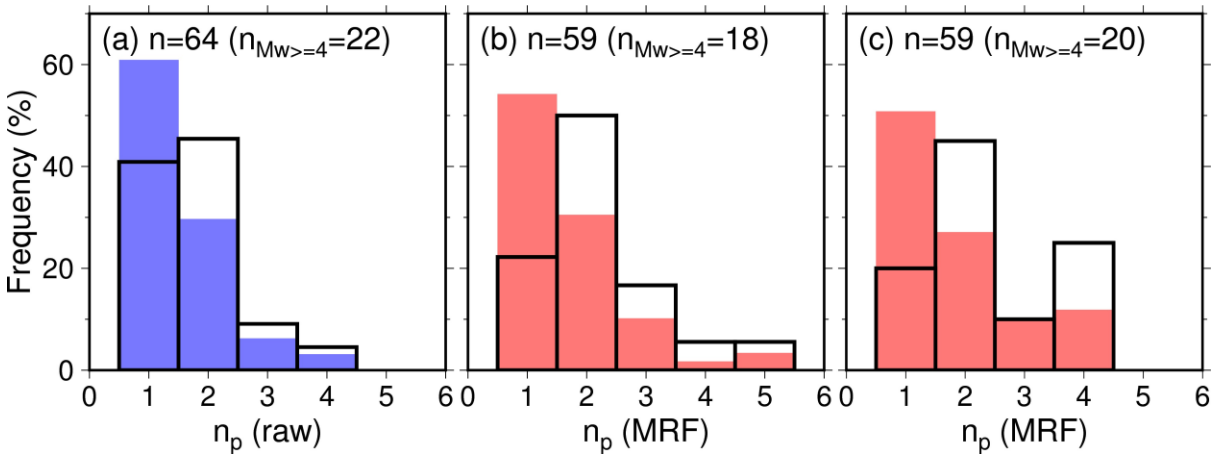

232

233

234 **Figure 4.** Histograms of the number of subevents estimated from the short-range
235 waveforms and MRFs. The colored bars represent all events, and the lines indicate events
236 with $M_w \geq 4.0$. (a) Direct P-wave, (b) MRFs obtained from the synthetic Green functions,
237 and (c) MRFs obtained from the EGFs.

238

239 Our direct waveform inspection was slightly affected by propagation. To remove
240 this contamination, we deconvolved the observed seismic waveforms using synthetic
241 Green's functions (Fig. S6). These theoretical waveforms were computed based on the
242 moment tensors and locations of each event. The hypocenter of each event was relocated
243 based on the same velocity structure used to calculate the synthetic waveforms (Hasegawa
244 et al., 1978), but from the hypocenters listed in the JMA catalog, with little change. For
245 the deconvolution, we used the iterative time-domain deconvolution algorithm of Ligorria
246 and Ammon (1999), which employs the method of Kikuchi and Kanamori (1982).
247 Deconvolution was performed with a non-negative constraint using a 20 Hz Butterworth
248 low-pass filter for stabilization, and results were obtained only when the recovery was
249 greater than 80%.

250 Figure 5 shows the derived MRFs of 59 events. They maintained the original
251 waveform shapes because of the minor impact of the propagation effect. Unlike the
252 original waveforms, they were slightly affected by instability during deconvolution (e.g.,
253 third or tenth event). However, counting the number of subevents from these MRFs, 27
254 out of 59 events had two or more subevents (46%; Fig. 4b), similar to the original

255 waveform result. Similarly, Fig. 4(c) shows the number of subevents when deconvolution
256 was performed using the waveforms of nearby small earthquakes as the EGF (Figs. S8).
257 The frequency band was set to f < 10 Hz to avoid the effects of finite durations of small
258 events. This result is also similar to the original result, in that 29 of the 59 (49 %) had
259 multiple pulses. The increased proportion of complex events in the post-deconvolution
260 results may be due in part to the effects of the deconvolution instability.
261
262

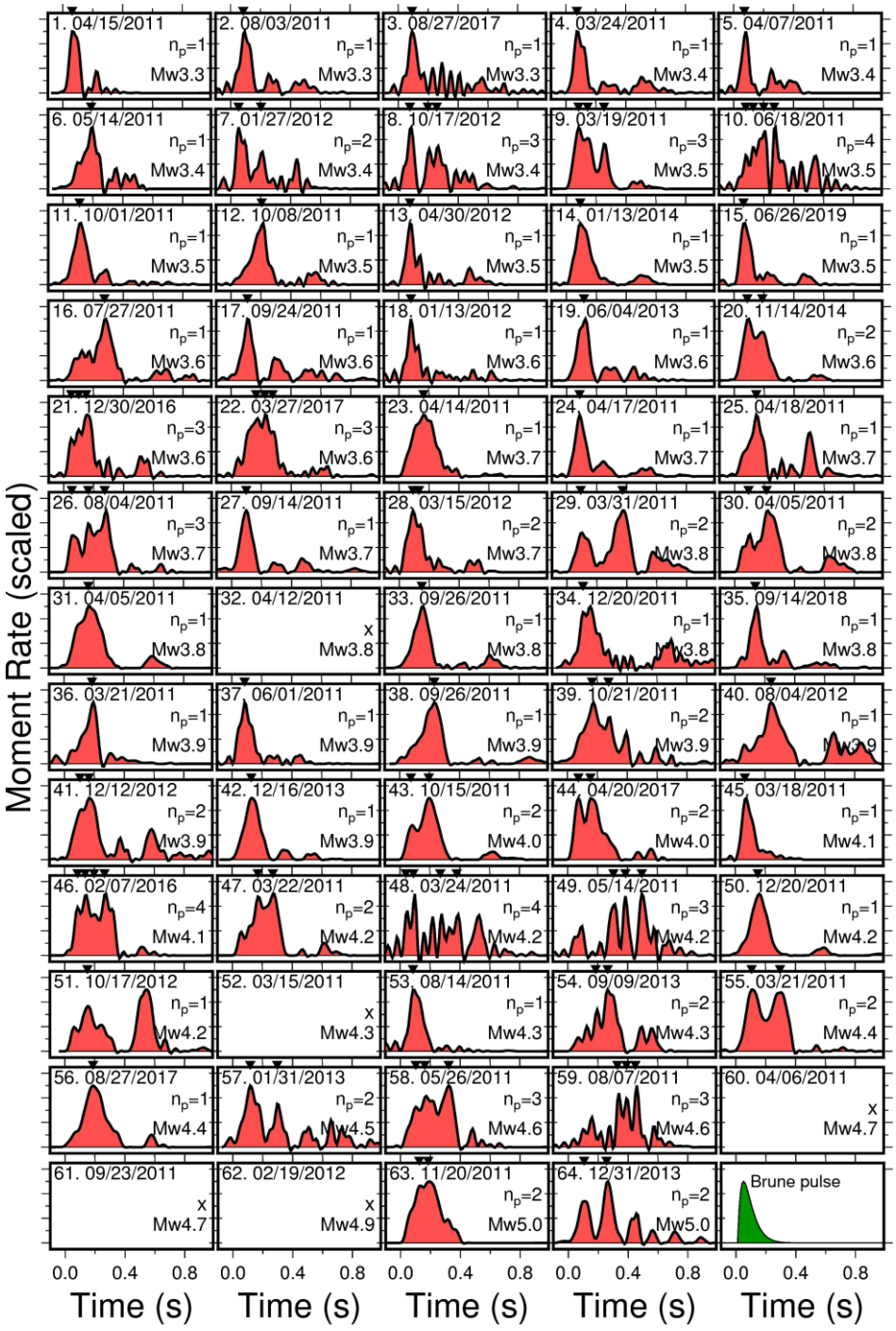

Fig. 5. Estimated moment-rate functions based on the deconvolution by synthetic waveforms. Triangles indicate the peaks of detected subevents. n_p indicates the number of detected subevents. An x mark indicates an event for which deconvolution did not work. The lower right panel shows the MRF of Brune's (1970) model.

Compiling the results of previous studies that examined a few small events with an extensive network suggests that it is common for small events to exhibit complexity (Ide,

2001; Yamada et al., 2005; Uchide & Ide, 2010; Taira et al., 2015; Wu et al., 2019). Yoshida and Kanamori (2023) studied more than 1700 Mw3-7 earthquakes in Japan based on the radiated energy enhancement factor (REEF; Ye et al., 2018). Their results showed that 30% of the analyzed events showed significant complexity (REEF>5), although the used frequency range was relatively narrow (up to approximately 7 Hz for Mw4 events). Those complex events tended to have significantly different source spectra from the ω^2-model, as expected (Madariaga, 1979). This study obtained consistent trends for 64 earthquakes by directly examining waveforms at a single station. Uchide and Imanishi (2016) examined the source spectra of M3.2-4 events in this region by spectral ratios and showed that many events deviate from the ω^2-model. Combined with our time-domain results, these may reflect a large number of complex events, even at this scale.

In the case of all three outcomes (Fig. 4), the number of subevents tends to be large for events with $M_w \geq 4$, which may be at least partly attributed to the temporal resolution of MRFs. With a given minimum resolvable duration (0.1 s) and sampling interval (0.01 s), resolving subevents for earthquakes with relatively short durations was difficult. This suggests that our complexity estimate may be underestimated; when measured only for Mw>4 earthquakes, 13 out of 22 events (59 %) showed multiple pulses.

Our estimated MRFs (Figs. 3, 4, and S8) exhibited various shapes. Some are simple and have a single pulse, similar to the source models often used for the estimation of the stress drop, such as those of Brune (1970), Sato and Hirasawa (1973), and Madariaga (1978). The green MRF in Figs. 3 and 5 show the MRF of Brune (1970) for comparison. However, even modest estimates show that approximately 30 % have multiple pulses that differ significantly from the above source models. The widely used source models produce erroneous results when applied to such complex events (Abercrombie, 2021; Liu et al., 2023). The present results suggest that methods that account for complexity, rather than those that assume a simple rupture pattern, are required to characterize even small earthquakes. One approach is to estimate the spatial variation of a spatially heterogeneous slip distribution/stress drop from seismic waveforms. However, the estimation uncertainties are very large owing to the degrees of freedom (Adams et al., 2016).

The radiated energy is a different physical quantity than the stress drop, but can

be estimated in principle directly from seismic waveform data without requiring a specific source model (e.g., Kanamori et al., 2020). Many source models have a one-to-one relationship between the radiated energy and stress drop through model-specific radiation efficiency. Ji et al. (2022) proposed estimating the stress drop based on radiated energy because radiation efficiency takes similar values in various source models. Snoke (1987) reported that estimating the stress drop from the apparent stress (moment-scale radiated energy multiplied by rigidity) is more stable. However, because radiation efficiency is not constant in reality (Venkataraman & Kanamori, 2004), it may be better to distinguish between stress drop and (moment-scaled) radiated energy and directly use radiated energy. Estimating the radiated energies of small earthquakes is not always straightforward because of strong propagation effects and frequency band limitations (Abercrombie, 2021). However, radiated energy is a quantity that can characterize small earthquakes regardless of their complexity and may be a suitable parameter for characterizing the source process of small earthquakes.

4. Conclusion

Short-range (< 8 km) seismic waveforms recorded at a downhole sensor surrounded by granite (Vp=5.4 km/s, Vs=3.2 km/s) clearly show the diversity in the complexity of the moment-rate functions for 64 Mw3.3-5.0 earthquakes. Even conservatively estimated, approximately 30% of the events had multiple pulses that differed significantly from simple source models. These results suggest that methods that account for complexity, rather than those that assume an a priori source process, are required to characterize even small earthquakes. Despite the difficulties in estimation, the present results suggest that using quantities such as radiated energy or moment-scale radiated energy is preferable as they can be estimated without assuming an a priori source process.

Acknowledgments

I am grateful to Hiroo Kanamori for highlighting the importance of this short-range observational data. We thank Toru Matsuzawa, Shunsuke Takemura, and Kentaro Emoto for discussing waveform modeling, which helped improve the manuscript. The figures

were created using GMT (Wessel & Smith, 1998). This study was financially supported by the JSPS KAKENHI (grant number JP 20K14569).

Open Research

Data Availability Statement

This study used hypocenter and arrival time data from the JMA-Unified Catalog (https://www.data.jma.go.jp/svd/eqev/data/bulletin/hypo.html). Waveforms were obtained from the NIED Hi-net website (https://www.hinet.bosai.go.jp/?LANG=en). They were collected and stored by NIED Hi-net (2019). The figures were created using GMT (Wessel and Smith, 1998).

342 **Reference**

343 Abercrombie, R. E. (1995). Earthquake source scaling relationships from -1 to 5 ML
344 using seismograms recorded at 2.5-km depth. *Journal of Geophysical Research*,
345 *100*(B12), 24015–24036. https://doi.org/10.1029/95jb02397

346 Abercrombie, R. E. (2021). Resolution and uncertainties in estimates of earthquake
347 stress drop and energy release. *Philosophical Transactions of the Royal Society A:*
348 *Mathematical, Physical and Engineering Sciences*, *379*(2196), 20200131.
349 https://doi.org/10.1098/rsta.2020.0131

350 Adams, M., Twardzik, C., & Ji, C. (2016). Exploring the uncertainty range of coseismic
351 stress drop estimations of large earthquakes using finite fault inversions.
352 *Geophysical Journal International*, *208*(1), 86–100.
353 https://doi.org/10.1093/gji/ggw374

354 Baltay, A., Prieto, G., & Beroza, G. C. (2010). Radiated seismic energy from coda
355 measurements and no scaling in apparent stress with seismic moment. *Journal of*
356 *Geophysical Research: Solid Earth (1978–2012)*, *115*(B8).
357 https://doi.org/10.1029/2009jb006736

358 Brocher, T. M. (2008). Key elements of regional seismic velocity models for long period
359 ground motion simulations. *Journal of Seismology*, *12*(2), 217–221.
360 https://doi.org/10.1007/s10950-007-9061-3

361 Brune, J. N. (1970). Tectonic stress and the spectra of seismic shear waves from
362 earthquakes. *J Geophys Res*, *75*(26), 4997–5009.
363 https://doi.org/10.1029/jb075i026p04997

364 Chounet, A., & Vallée, M. (2018). Global and Interregion Characterization of
365 Subduction Interface Earthquakes Derived From Source Time Functions Properties.

Journal of Geophysical Research: Solid Earth, *123*(7), 5831–5852. https://doi.org/10.1029/2018jb015932

Courboulex, F., Virieux, J., Deschamps, A., Gibert, D., & Zollo, A. (1996). Source investigation of a small event using empirical Green's functions and simulated annealing. *Geophysical Journal International*, *125*(3), 768–780. https://doi.org/10.1111/j.1365-246x.1996.tb06022.x

Denolle, M. A., & Shearer, P. M. (2016). New perspectives on self-similarity for shallow thrust earthquakes. *Journal of Geophysical Research: Solid Earth*, *121*(9), 6533–6565. https://doi.org/10.1002/2016jb013105

Duputel, Z., Tsai, V. C., Rivera, L., & Kanamori, H. (2013). Using centroid time-delays to characterize source durations and identify earthquakes with unique characteristics. *Earth and Planetary Science Letters*, *374*, 92–100. https://doi.org/10.1016/j.epsl.2013.05.024

Eshelby, J. D. (1957). The determination of the elastic field of an ellipsoidal inclusion, and related problems. *Proceedings of the Royal Society of London. Series A, Mathematical and Physical Sciences*, 376–396. https://doi.org/10.1098/rspa.1983.0054

Harrington, R. M., & Brodsky, E. E. (2009). Source Duration Scales with Magnitude Differently for Earthquakes on the San Andreas Fault and on Secondary Faults in Parkfield, CaliforniaSource Duration Scales with Magnitude Differently on the San Andreas Fault and on Secondary Faults. *Bulletin of the Seismological Society of America*, *99*(4), 2323–2334. https://doi.org/10.1785/0120080216

Hartzell, S. H. (1978). Earthquake aftershocks as Green's functions. *Geophysical Research Letters*, *5*(1), 1–4. https://doi.org/10.1029/GL005i001p00001

Hasegawa, A., Umino, N., & Takagi, A. (1978). Double-planed structure of the deep seismic zone in the northeastern Japan arc. *Tectonophysics*, *47*(1–2), 43–58. https://doi.org/10.1016/0040-1951(78)90150-6

Holmgren, J. M., Atkinson, G. M., & Ghofrani, H. (2019). Stress Drops and Directivity of Induced Earthquakes in the Western Canada Sedimentary BasinStress Drops and Directivity of Induced Earthquakes in the Western Canada Sedimentary Basin. *Bulletin of the Seismological Society of America*, *109*(5), 1635–1652. https://doi.org/10.1785/0120190035

Hough, S. E. (1997). Empirical Green's function analysis: Taking the next step. *Journal of Geophysical Research: Solid Earth*, *102*(B3), 5369–5384. https://doi.org/10.1029/96jb03488

Houston, H., Benz, H. M., & Vidale, J. E. (1998). Time functions of deep earthquakes from broadband and short-period stacks. *Journal of Geophysical Research: Solid Earth*, *103*(B12), 29895–29913. https://doi.org/10.1029/98jb02135

Hutchings, L., & Viegas, G. (2012). Application of Empirical Green's Functions in Earthquake Source, Wave Propagation and Strong Ground Motion Studies. *Earthquake Research and Analysis: New Frontiers in Seismology*.

Ide, S. (2001). Complex source processes and the interaction of moderate earthquakes during the earthquake swarm in the Hida-Mountains, Japan, 1998. *Tectonophysics*, *334*(1), 35–54. https://doi.org/10.1016/S0040-1951(01)00027-0

Ide, S., & Beroza, G. C. (2001). Does apparent stress vary with earthquake size? *Geophysical Research Letters*, *28*(17), 3349–3352. https://doi.org/10.1029/2001GL013106

Ji, C., Archuleta, R. J., & Wang, Y. (2022). Variability of Spectral Estimates of Stress Drop Reconciled by Radiated Energy. *Bulletin of the Seismological Society of America*. https://doi.org/10.1785/0120210321

Kanamori, H., & Anderson, D. (1975). Theoretical basis of some empirical relations in seismology. *Bulletin of the Seismological Society of America*, *65*(5), 1073–1095. Retrieved from http://bssa.geoscienceworld.org/content/65/5/1073.short

Kanamori, H., Mori, J., & Heaton, T. H. (1990). THE 3 DECEMBER 1988, PASADENA EARTHQUAKE (ML = 4.9) RECORDED WITH THE VERY BROADBAND SYSTEM IN PASADENA. *Bulletin of the Seismological Society of America*.

Kanamori, H., Ross, Z. E., & Rivera, L. (2020). Estimation of radiated energy using the KiK-net downhole records - Old method for modern data. *Geophysical Journal International*, *221*(2), 1029–1042. https://doi.org/10.1093/gji/ggaa040

Kaneko, Y., & Shearer, P. M. (2014). Seismic source spectra and estimated stress drop derived from cohesive-zone models of circular subshear rupture. *Geophysical Journal International*, *197*(2), 1002–1015. https://doi.org/10.1093/gji/ggu030

Kikuchi, M., & Ishida, M. (1993). Source retrieval for deep local earthquakes with broadband records. *Bulletin of the Seismological Society of America*, *83*(6), 1855–1870. https://doi.org/10.1785/bssa0830061855

Kikuchi, M., & Kanamori, H. (1982). Inversion of complex body waves -. *Bulletin - Seismological Society of America*, *72*(2), 491–506. https://doi.org/10.1785/bssa0810062335

Kubo, A., Fukuyama, E., Kawai, H., & Nonomura, K. (2002). NIED seismic moment tensor catalogue for regional earthquakes around Japan: quality test and application. *Tectonophysics*, *356*(1–3), 23–48. https://doi.org/10.1016/S0040-1951(02)00375-X

Kwiatek, G. (2008). Relative source time functions of seismic events at the Rudna copper mine, Poland: estimation of inversion uncertainties. *Journal of Seismology*, *12*(4), 499–517. https://doi.org/10.1007/s10950-008-9100-8

Ligorría, J. P., & Ammon, C. J. (1999). Iterative deconvolution and receiver-function estimation. *Bulletin of the Seismological Society of America*, *89*(5), 1395–1400.

Lin, Y.-Y., Ma, K.-F., Kanamori, H., Song, T.-R. A., Lapusta, N., & Tsai, V. C. (2016). Evidence for non-self-similarity of microearthquakes recorded at a Taiwan borehole seismometer array. *Geophysical Journal International*, *206*(2), 757–773. https://doi.org/10.1093/gji/ggw172

Liu, C., Lay, T., Wang, R., Taymaz, T., Xie, Z., Xiong, X., et al. (2023). Complex multi-fault rupture and triggering during the 2023 earthquake doublet in southeastern Türkiye. *Nature Communications*, *14*(1), 5564. https://doi.org/10.1038/s41467-023-41404-5

Malagnini, L., Mayeda, K., Nielsen, S., Yoo, S.-H., Munafo', I., Rawles, C., & Boschi, E. (2014). Scaling Transition in Earthquake Sources: A Possible Link Between Seismic and Laboratory Measurements. *Pure and Applied Geophysics*, *171*(10), 2685–2707. https://doi.org/10.1007/s00024-013-0749-8

Mayeda, K., & Walter, W. R. (1996). Moment, energy, stress drop, and source spectra of western United States earthquakes from regional coda envelopes. *Journal of Geophysical Research B: Solid Earth*, *101*(5), 11195–11208. https://doi.org/10.1029/96jb00112

Mueller, C. S. (1985). Source pulse enhancement by deconvolution of an empirical Green's function. *Geophysical Research Letters*, *12*(1), 33–36. https://doi.org/10.1029/gl012i001p00033

462 NIED. (2019). NIED Hi-net, National Research Institute for Earth Science and Disaster
463 Resilience. https://doi.org/10.17598/NIED.0003

464 Nishitsuji, Y., & Mori, J. (2014). Source parameters and radiation efficiency for
465 intermediate-depth earthquakes in Northeast Japan. *Geophysical Journal*
466 *International*, *196*(2), 1247–1259. https://doi.org/10.1093/gji/ggt458

467 Pennington, C. N., Wu, Q., Chen, X., & Abercrombie, R. E. (2023). Quantifying rupture
468 characteristics of microearthquakes in the Parkfield Area using a high-resolution
469 borehole network. *Geophysical Journal International*, *233*(3), 1772–1785.
470 https://doi.org/10.1093/gji/ggad023

471 Pérez-Campos, X., & Beroza, G. C. (2001). An apparent mechanism dependence of
472 radiated seismic energy. *Journal of Geophysical Research: Solid Earth*, *106*(B6),
473 11127–11136. https://doi.org/10.1029/2000jb900455

474 Prejean, S. G., & Ellsworth, W. L. (2001). Observations of Earthquake Source
475 Parameters at 2 km Depth in the Long Valley Caldera, Eastern California. *Bulletin*
476 *of the Seismological Society of America*, *91*(2), 165–177.
477 https://doi.org/10.1785/0120000079

478 Sato, T., & Hirasawa, T. (1973). Body wave spectra from propagating shear cracks.
479 *Journal of Physics of the Earth*. https://doi.org/10.4294/jpe1952.21.415

480 Snoke, J. A. (1987). STABLE DETERMINATION OF (BRUNE) STRESS DROPS.
481 *Bulletin of the Seismological Society of America*.

482 Taira, T., Dreger, D. S., & Nadeau, R. M. (2015). Rupture process for micro-
483 earthquakes inferred from borehole seismic recordings. *International Journal of*
484 *Earth Sciences*, *104*(6), 1499–1510. https://doi.org/10.1007/s00531-015-1217-8

485 Takahashi, T., Sato, H., Ohtake, M., & Obara, K. (2005). Scale dependence of apparent
486 stress for earthquakes along the subducting pacific plate in northeastern Honshu,

Japan. *Bulletin of the Seismological Society of America*, *95*(4), 1334–1345. https://doi.org/10.1785/0120040075

Tanioka, Y., & Ruff, L. J. (1997). Source Time Functions. *Seismological Research Letters*, *68*(3), 386–400. https://doi.org/10.1785/gssrl.68.3.386

Uchide, T., & Ide, S. (2010). Scaling of earthquake rupture growth in the Parkfield area: Self-similar growth and suppression by the finite seismogenic layer. *Journal of Geophysical Research: Solid Earth (1978–2012)*, *115*(B11). https://doi.org/10.1029/2009jb007122

Vallée, M., J. Charléty, A. M. G. Ferreira, B. Delouis, J. Vergoz (2011). SCARDEC: a new technique for the rapid determination of seismic moment magnitude, focal mechanism and source time functions for large earthquakes using body-wave deconvolution. *GEOPHYSICAL JOURNAL INTERNATIONAL*, *184*, 338-358. https://doi.org/10.1111/j.1365-246X.2010.04836.x

Venkataraman, A., & Kanamori, H. (2004). Observational constraints on the fracture energy of subduction zone earthquakes. *Journal of Geophysical Research: Solid Earth*, *109*(5). https://doi.org/10.1029/2003JB002549

Wessel, P., & Smith, W. H. F. (1998). New, improved version of generic mapping tools released. *Eos, Transactions American Geophysical Union*, *79*(47), 579–579. https://doi.org/10.1029/98EO00426

Wu, Q., Chen, X., & Abercrombie, R. E. (2019). Source Complexity of the 2015 Mw 4.0 Guthrie, Oklahoma Earthquake. *Geophysical Research Letters*, *46*(9), 4674–4684. https://doi.org/10.1029/2019gl082690

Yamada, T., Mori, J. J., Ide, S., Kawakata, H., Iio, Y., & Ogasawara, H. (2005). Radiation efficiency and apparent stress of small earthquakes in a South African

gold mine. *Journal of Geophysical Research: Solid Earth (1978–2012)*, *110*(B1). https://doi.org/10.1029/2004jb003221

Yamaya, L., Mochizuki, K., Akuhara, T., Takemura, S., Shinohara, M., & Yamada, T. (2022). CMT inversion for small-to-moderate earthquakes applying to dense short-period OBS array at off Ibaraki region. *Earth, Planets and Space*, *74*(1), 164. https://doi.org/10.1186/s40623-022-01721-3

Ye, L., Kanamori, H., & Lay, T. (2018). Global variations of large megathrust earthquake rupture characteristics. *Science Advances*, *4*(3), eaao4915. https://doi.org/10.1126/sciadv.aao4915

Ye, L., Lay, T., Kanamori, H., & Rivera, L. (2016). Rupture characteristics of major and great (Mw ≥ 7.0) megathrust earthquakes from 1990 to 2015: 1. Source parameter scaling relationships. *Journal of Geophysical Research: Solid Earth*. https://doi.org/10.1002/2015JB012426

Yoshida, K., & Kanamori, H. (2023). Time-domain source parameter estimation of M w 3–7 earthquakes in Japan from a large database of moment-rate functions. *Geophysical Journal International*. https://doi.org/10.1093/gji/ggad068

Yoshida, K., Hasegawa, A., & Okada, T. (2015). Spatially heterogeneous stress field in the source area of the 2011 Mw 6.6 Fukushima-Hamadori earthquake, NE Japan, probably caused by static stress change. Geophysical Journal International, 201(2), 1062–1071. https://doi.org/10.1093/gji/ggv068

Yoshida, K., Saito, T., Emoto, K., Urata, Y., & Sato, D. (2019). Rupture directivity, stress drop, and hypocenter migration of small earthquakes in the Yamagata-Fukushima border swarm triggered by upward pore-pressure migration after the 2011 Tohoku-Oki earthquake. *Tectonophysics*, *769*. https://doi.org/10.1016/j.tecto.2019.228184

536 Yoshida, K., Hasegawa, A., Yoshida, T., & Matsuzawa, T. (2019). Heterogeneities in
537 Stress and Strength in Tohoku and Its Relationship with Earthquake Sequences
538 Triggered by the 2011 M9 Tohoku-Oki Earthquake. *Pure and Applied Geophysics*,
539 *176*(3), 1335–1355. https://doi.org/10.1007/s00024-018-2073-

540

541